Two-step sequential bio-oxidation of arsenopyrite catalyzed by a mesophilic bacterium eliminates hazardous Fe(III)/As-bearing products and enhances mineral dissolution

Chen, H-R., Li, Q., Zhao, X-J., Zhang, D-R. & Pakostova, E

Original citation & hyperlink:
Chen, H-R, Li, Q, Zhao, X-J, Zhang, D-R & Pakostova, E 2023, 'Two-step sequential bio-oxidation of arsenopyrite catalyzed by a mesophilic bacterium eliminates hazardous Fe(III)/As-bearing products and enhances mineral dissolution', Chemical Engineering Journal, vol. 462, 142259. https://doi.org/10.1016/j.cej.2023.142259

DOI [10.1016/j.cej.2023.142259
ISSN 1385-8947

Publisher: Elsevier

Two-step sequential bio-oxidation of arsenopyrite catalyzed by a mesophilic bacterium eliminates hazardous Fe(III)/As-bearing products and enhances mineral dissolution

Hong-Rui Chen[a], Qian Li[a], Xiao-Juan Zhao[b], Duo-Rui Zhang[a,*], Eva Pakostova[c]

[a] School of Minerals Processing and Bioengineering, Central South University, Changsha 410083, China

[b] Beijing Synchrotron Radiation Facility, Institute of High Energy Physics, Chinese Academy of Sciences, Beijing 100049, China

[c] Centre for Manufacturing and Materials, Coventry University, Coventry CV1 5FB, UK

* Corresponding author: e-mail: drzhang@csu.edu.cn

Abstract: Arsenopyrite (FeAsS) is one of the most typical As-bearing sulfide minerals and bio-oxidation of arsenopyrite is a process of particular scientific interest, due to its broad application in gold mineral processing as well as the release of toxic As. This study aimed to enhance the dissolution of arsenopyrite (as well as of Fe(III)/As-bearing oxidation products) *via* a sequential two-step process comprising aerobic bio-oxidation and reductive dissolution under anaerobic conditions, both catalyzed by *Acidithiobacillus* (*At.*) *thiooxidans* DSM 504: (i) during aerobic bio-oxidation, 67.7 and 64.9% As was extracted from arsenopyrite in a basal salts medium (BSM) and acid mine drainage (AMD) respectively. A double passivation layer (comprising jarosite and a dense outer layer) formed on the mineral surface in BSM, inhibiting further bio-oxidation, while an oxidation layer with a more permeable amorphous nanosheet structure (composing of tooeleite) was formed in AMD. (ii) Subsequently, the reductive dissolution process effectively eliminated the double passivation layer (composed of S^0, amorphous ferric arsenate, K-jarosite, tooeleite, and scorodite), with 47.2 and 91.9% Fe reduced in 16 days of anaerobic bio-oxidation of S^0 and $S_2O_3^{2-}$, respectively. The proposed two-step bio-oxidation process has the potential to contribute to the development of improved extractive technologies, and avoid the accumulation of unstable As pollution sources. Additionally, the data indicate that a replacement of growth media with AMD could reduce the elevated costs of the technology capable of alternating aerated and anoxic bio-oxidation stages.

Keywords: Arsenopyrite; Bio-oxidation; Reductive dissolution; *Acidithiobacillus thiooxidans*; Acid mine drainage; Sulfur oxidation

1. Introduction

Arsenopyrite (FeAsS) is one of the most abundant auriferous sulfidic ores. Gold (Au) is often associated with the mineral in the form of micro-fine particles, which complicates the extraction of the precious metal (Cabri et al., 2000; Vikentyev 2015). Several approaches have been used to promote the dissolution of arsenopyrite, including pyrometallurgy flotation (Brittan, 1995), pressure oxidation (Ng et al., 2022), and leaching with strong inorganic acids (Rogozhnikov et al., 2021). The above techniques are costly (due to a high energy consumption and equipment requirements), and present serious environmental hazards (caused by large amounts of potentially hazardous wastes and emissions generated, and/or the use of harsh chemicals).

Bioleaching (and bio-oxidation) is considered a cost-effective and environmentally sustainable alternative to the traditional extractive techniques, and is suitable for the recovery of valuable metals from a range of minerals and waste materials (Roberto and Schippers, 2022; Zeng et al., 2016; Brierley and Brierley, 2013). A number of acidophilic Fe- and/or S-oxidizing bacteria that are commonly detected in acidic environments (such as *Acidithiobacillus* spp.) have been applied in arsenopyrite bio-oxidation (Ramírez-Aldaba et al., 2016; Dave et al., 2008). Under aerobic conditions, biogenic Fe^{3+} and H_2SO_4 are the primary chemical agents mediating the dissolution of arsenopyrite. To further enhance the dissolution process, different culture media (e.g., 9K, basal salts medium (BSM)) and effectors have been studied, with the latter including minerals (e.g., pyrite, Deng et al., 2020), organic compounds (e.g., humic acid, Zhang et al., 2020), and metal ions (e.g., Fe^{3+}, Ag^{+}, Cu^{2+}, etc) (Pathak et al., 2017).

Arsenopyrite bio-oxidation is a (bio)chemically complex process that is further affected by the presence of metal ions (additions of which increase the mineral processing costs). Additional metal ions may support bacterial growth, but can also promote the accumulation of a variety of secondary products, thus affecting the mobility of aqueous chemical species (Lengke et al., 2009) and potentially inhibiting the dissolution of arsenopyrite through the formation of a passivation layer (Zhang et al., 2021; Tabelin et al., 2020). Inorganic ions commonly used in culture media (especially, K^+ and NH_4^+) enhance the formation of K-jarosite and ammoniojarosite, which can lead to immobilization of metal(loid)s (including As) *via* adsorption and/or co-precipitation (Ryu and Kim, 2022). The As-rich by-products are often generated in large amounts, and are commonly stored in tailings storage facilities or deposited in heaps (Shaw et al., 2013). Such mine waste storage practices present a great threat to the surrounding environment, particularly due to the low stability of the wastes, which may significantly contribute to the generation of AMD rich in As.

The potential of many microorganisms (including fungi, archaea, and heterotrophic and autotrophic bacteria) has been explored for reductive dissolution of Fe(III) minerals (Sharma and Eisele, 2021; Marrero et al., 2015; Osorio et al., 2013). Jarosites, which are among the most common by-products and metal(loid) sinks in bioleaching processes, can be dissolved *via* anaerobic microbial processes that utilize organic matter, hydrogen, or reduced inorganic sulfur compounds as electron donors (Chen et al., 2022; Castro et al., 2013; Ohmura et al., 2002). However, limited knowledge exists about microbially catalyzed reductive dissolution of bio-oxidized arsenopyrite residues

(BOARs) that accumulate during aerobic bioleaching processes. Besides S^0 and As-bearing jarosites, these processes generate large amounts of As(III/V)/Fe(III)-bearing phases (e.g., amorphous ferric arsenate and scorodite).

This study is the first to describe efficient dissolution of arsenopyrite and its secondary products through sequential bio-oxidation comprising an aerobic and an anaerobic step, both catalyzed by a single strain of *At. thiooxidans*. The main aims of the novel approach were to enhance arsenopyrite dissolution and mitigate the generation of potentially hazardous Fe(III)/As-bearing oxidation products. Compared to previous studies, the use of an improved (Fe-free) growth medium lowered the accumulation of secondary products, and would significantly reduce process costs in larger-scale operations. As part of the research, the promising potential of AMD to enhance arsenopyrite bio-oxidation was also evaluated. On a larger scale, the findings could contribute to the development of novel mineral processing technologies with improved leaching kinetic, as well as reduced costs and environmental impacts.

2. Materials and methods

2.1. Bacterial strain and culture conditions

The bacterial strain *At. thiooxidans* DSM 504, capable of anaerobic Fe^{3+} reduction coupled to S oxidation (as postulated by Chen et al., 2022), was obtained from the Key Laboratory of Biometallurgy of the Ministry of Education of China, Changsha, China. To adapt the strain to elevated As concentrations that occur during arsenopyrite bio-oxidation, 10 g/L arsenopyrite was added to a basal salts medium (BSM; pH 2.0,

adjusted using 5 M H_2SO_4) containing (in g/L): $(NH_4)_2SO_4$, 3.0; $MgSO_4$, 0.5; K_2HPO_4, 0.5; KCl, 0.1; $Ca(NO_3)_2$, 0.01. Prior to the adaption, BSM was autoclaved (121 ℃, 30 min) and arsenopyrite was sterilized by washing in alcohol (for 10 min), followed by ultrasonic cleaning (three times 1 min), triple rinsing in water, and drying (150 ℃, > 6 hours). Finally, the adaption flask was inoculated with *At. thiooxidans* and cultivated at 30 ℃ and 170 rpm.

2.2. Materials

Arsenopyrite used in the bio-oxidation experiments was collected from a Carlin type Au deposit in the Guangxi province, China. The mineral sample was ground and sieved (using a 200-400 mesh) to obtain a fine particle fraction (38-75 μm diameter). The X-ray diffraction (XRD) analysis of the mineral sample confirmed the main phase comprised arsenopyrite (Fig. S1). An elemental composition analysis by inductively coupled plasma-atomic emission spectroscopy (ICP-AES) showed the contents of Fe, As, and S in the arsenopyrite were 33.3, 43.9, and 19.54 wt.%, respectively. Besides the major constituents, minor contents of the following elements were detected (in wt.%): 0.98 Al, 0.61 Si, 0.39 Cu, and 0.24 Ca.

To explore the feasibility of using AMD as a growth medium to further reduce mineral processing costs, aerobic bio-oxidation of arsenopyrite by *At. thiooxidans* in AMD, besides BSM, was investigated. The AMD sample was collected from the Dabaoshan Mine area (24°34′28"N, 113°43′42"), which is the largest polymetallic mine in South China (Chen et al., 2020). The main dissolved elements detected in AMD were

(in g/L): 0.67 Fe, 0.37 Ca, 0.41 Al, 0.23 Zn, 0.11 Mn, 0.06 Na, 0.04 Cu, 0.04 Si, and 0.02 K. The bulk pH and oxidation reduction potential (ORP) values determined in the collected AMD were 2.03 and +537 mV, respectively. Prior to use in bio-oxidation experiments, the AMD sample was centrifuged (12,000 g, 10 min) and filtered (0.22 μm), to remove fine materials and bacteria.

2.3. Sequential bio-oxidation of arsenopyrite by At. thiooxidans

2.3.1. Aerobic bioleaching

Aerobic bioleaching experiments were carried out in 250 mL Erlenmeyer flasks containing 10 g/L sterile arsenopyrite in 100 mL sterilized BSM (pH 2.0) or AMD. *At. thiooxidans* was inoculated at an initial concentration of 1.2×10^8 cells/mL. The bioleaching assays were cultivated in a shaking incubator at 30 ℃ and 170 rpm. Un-inoculated flasks served as abiotic controls. All assays were performed in triplicate, and kinetic parameters were regularly monitored. After 15 days of aerobic bioleaching, the solid residues were collected and analyzed for composition. Additionally, the accumulated Fe(III)-rich solids from the BSM assay (below referred to as BOAR) were used in the following reductive dissolution step.

2.3.2. Anaerobic sulfur bio-oxidation coupled to BOAR reductive dissolution

To determine the ability of *At. thiooxidans* to dissolve BOAR and to investigate the mechanism of Fe reduction coupled to S bio-oxidation, the subsequent anaerobic reduction step was performed in a separate system, which prevented inhibition of the

bacterium by elevated concentrations of oxidation products. The reductive dissolution was performed in 150 mL serum bottles containing 10 g/L BOAR in 50 mL sterile BSM (pH 2.0). The serum bottles were inoculated with *At. thiooxidans* to an initial cell density of 1.2×10^8 cells/mL. Two inorganic sulfur compounds, S^0 or $Na_2S_2O_3$ (at concentrations corresponding to 1, 2, and 3 g sulfur/L), were used as electron donors for the anaerobic growth of *At. thiooxidans* with Fe^{3+} (supplied in BOAR) serving as electron acceptor. The assays were performed in duplicate, and incubated in a thermostatic shaker at 30 ℃ and 170 rpm. Control flasks were carried out without sulfur compounds under similar conditions as described above.

2.4. Analytical methods

To monitor the kinetics of the bio-oxidation processes, liquid samples were collected from the assays every 1 to 2 days. The pH and ORP values were determined in the samples using a pH meter (PB-10, Beijing Sartorius Scientific Instrument Co. Ltd., China) and potentiometer (PHSJ-4F, Shanghai Inesa Scientific Instruments Co. Ltd., China), with a reference Ag/AgCl electrode. The concentrations of total soluble iron ($[Fe^T]_{aq}$) and Fe^{3+} ($[Fe^{3+}]_{aq}$) during aerobic bioleaching were determined using the 5-sulfosalicylic acid colorimetric method (Karamanev et al., 2002). In samples collected from the anaerobic assays, $[Fe^{2+}]_{aq}$ and $[Fe^T]_{aq}$ were measured using the ferrozine method (Lovley and Phillips, 1987). The concentration of total dissolved As ($[As^T]_{aq}$) was analyzed using ICP-MS (7700x, Agilent Technologies, USA) and soluble As speciation ($[As(III)]_{aq}$ and $[As(V)]_{aq}$) was determined using high-performance liquid

chromatography combined with ICP-MS (HPLC-ICP-MS) using an anion exchange column. The concentration of sulfate ($[SO_4^{2-}]_{aq}$) in liquid samples was analyzed using the barium sulfate turbidimetric method (Zhu et al., 2011).

Prior to characterization of bioleaching residues, the solids were gently washed twice using deionized water (with pH adjusted to that of the leaching solution), kept at -80 ℃ for more than 12 hours and then freeze-dried. The surface morphology and elemental composition of the solid samples were investigated using field-emission scanning electron microscopy (FE-SEM; TESCAN MIRA3, Czech Republic). The sample mineralogy was determined using X-ray diffraction (XRD; D8 ADVANCE, Bruker, Germany). The valence state of sulfur was determined by X-ray photoelectron spectroscopy (XPS; K-Alpha 1063, Thermo Fisher Scientific, USA), using Al Kα X-ray as an excitation source. The speciation of As and Fe in solid samples was determined using As K-edge and Fe L-edge X-ray absorption near edge structure (XANES) spectroscopy, conducted in 1W2B and 4B7B beamlines respectively at Beijing Synchrotron Radiation Facility (BSRF), Beijing, China. Athena software was used for the normalization of XANES spectra and linear combination fitting (LCF) analysis, and the goodness of fit was evaluated by the reduced chi-square value (Ravel and Newville, 2005; Datta et al., 2012).

3. Results and discussion

3.1. Kinetics of arsenopyrite bioleaching under aerobic conditions

The changes in pH during aerobic bioleaching of arsenopyrite were affected mainly

by S and Fe oxidation catalyzed by *At. thiooxidans,* but also by the formation of secondary products passivating the mineral surface. The pH value in the BSM assay (Fig. 1a) increased slowly at the beginning and this increase accelerated after day 2 due to rapid oxidation of Fe^{2+} (Eq. (1)). A maximum pH value (~2.4) was reached on day 6, followed by a decrease. In the AMD assay, a decrease in both pH (Fig. 1a) and ORP (Fig. 1b; mainly determined by $[Fe^{3+}]_{aq}/[Fe^{2+}]_{aq}$, Zhang et al., 2015) was observed in the first 2 days, due to the attack of Fe^{3+} on arsenopyrite surface generating H^+ and Fe^{2+} (Eq. (2)). Similar changes in pH and ORP were observed in the sterile controls (Fig. S2a, b). An additional supply of iron (which undergoes active redox cycling in arsenopyrite bioleaching systems) present in AMD, explained a higher cell density in AMD compared to BSM (Fig. 1c). The main cause of the pH decrease observed after 6 days in both BSM and AMD was the generation of H^+ during S bio-oxidation (Eq. (3); sulfate production showed in Fig. S3), as well as during the formation of Fe(III)- and/or As-bearing phases such as jarosites ($MFe_3(SO_4)_2(OH)_6$, where M is K^+, NH_4^+, Na^+, or H_3O^+) (Eq. (4)) and tooeleite ($Fe_6(AsO_3)_4(SO_4)(OH)_4{\cdot}4H_2O$) (Eq. (5)) (shown in Fig. 3).

$$4Fe^{2+} + 4H^+ + O_2 \xrightarrow{biotic} 4Fe^{3+} + 2H_2O \quad (1)$$

$$5Fe^{3+} + FeAsS + 3H_2O \xrightarrow{abiotic} 6Fe^{2+} + H_3AsO_3 + S^0 + 3H^+ \quad (2)$$

$$2S + 3O_2 + 2H_2O \xrightarrow{biotic} 2{SO_4}^{2-} + 4H^+ \quad (3)$$

$$3Fe^{3+} + 2{SO_4}^{2-} + M^+ + 6H_2O \xrightarrow{abiotic} MFe_3(SO_4)_2(OH)_6 + 6H^+ \quad (4)$$

$$6Fe^{3+} + 4{AsO_3}^{3-} + {SO_4}^{2-} + 8H_2O \xrightarrow{abiotic} Fe_6(AsO_3)_4(SO_4)(OH)_4 \cdot 4H_2O + 4H^+ \quad (5)$$

Fig. 1d shows that $[Fe^T]_{aq}$ in both BSM and AMD biotic assays gradually increased due to progressing dissolution of arsenopyrite. In the BSM assay, soluble Fe occurred mainly as Fe^{3+} during the whole bioleaching process, and reached a maximum concentration (1.13 g/L) on day 9, followed by a slight decrease due to precipitation of Fe(III) minerals. In the AMD assay, Fe^{2+} was the dominant form of soluble Fe during the first 4 days of arsenopyrite bioleaching, while no Fe^{2+} was detected after day 6. The extensive iron oxidation affected the color of the AMD assay, turning it darker yellow compared to the BSM assay (shown in Fig. 1b). No significant increase in $[Fe^T]_{aq}$ or iron oxidation were detected in the BSM and AMD abiotic assays during the time course of the incubation (Fig. S2c). The above results confirmed the catalytic role of *At. thiooxidans* in S/Fe oxidation and arsenopyrite dissolution under acidic conditions, as described by others (Rohwerder et al., 2003).

Fig. 1e shows $[As^T]_{aq}$ gradually increased with the progression of aerobic bioleaching of arsenopyrite, with As(III) dominating in both (BSM and AMD) assays. Fe^{3+} present in AMD promoted arsenopyrite dissolution, leading to enhanced release of As in the first 7 days, compared to BSM. However, from day 9, $[As^T]_{aq}$ in the AMD assay was lower than that in BSM, likely due to precipitation of tooeleite facilitated by the elevated Fe(III)/As(III) ratio (Chai et al., 2016; Duquesne et al., 2003). The maximum rates of As bioleaching from arsenopyrite were 67.7 and 64.9% in the BSM and AMD assays respectively, determined on day 15 (Fig. 1f), with the As solubilization rate in AMD likely to be underestimated, due to rapid precipitation of tooeleite (discussed below). In any case, these values were significantly higher than those in

abiotic controls (which reached 5.1 and 7.6% in BSM and AMD respectively; Fig. 1f and Fig. S2d).

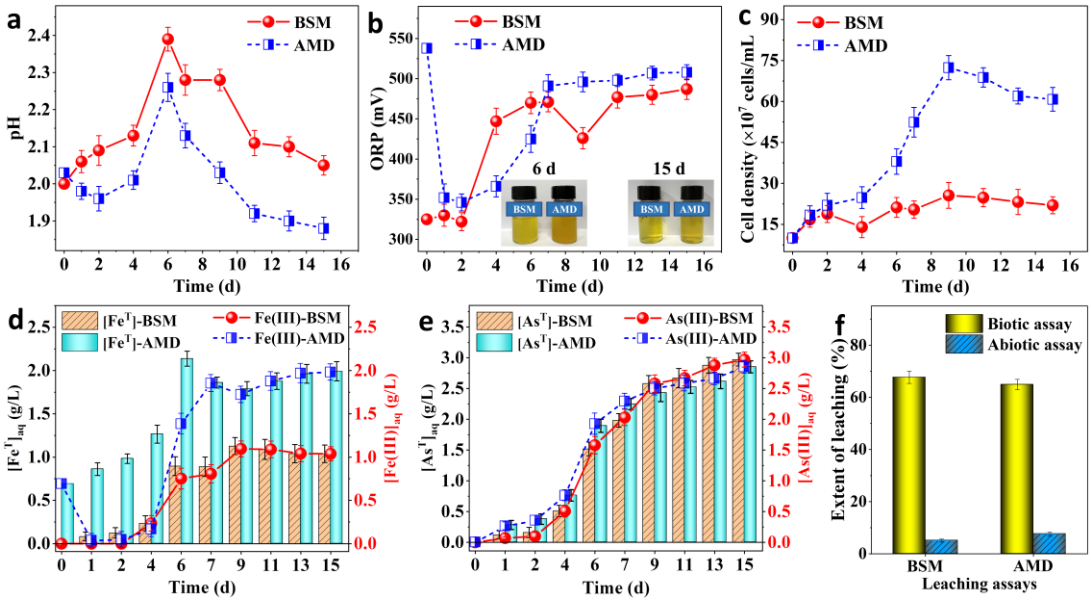

Fig. 1. Changes in (a) pH, (b) ORP, (c) cell density, (d) $[Fe^T]_{aq}$ and $[Fe^{3+}]_{aq}$, and (e) $[As^T]_{aq}$ and $[As(III)]_{aq}$ during aerobic bioleaching of arsenopyrite catalyzed by *At. thiooxidans* in BSM and AMD; and (f) the proportions of As in solution (reflecting both arsenopyrite dissolution and subsequent precipitation of secondary minerals) in biotic and abiotic assays.

3.2. Characterization of solid products after aerobic bioleaching of arsenopyrite

The SEM results show that after 4 days of aerobic bioleaching, a thin fine oxidation layer was formed on the surface of arsenopyrite in both BSM (Fig. 2a) and AMD (Fig. 2e). It is likely that this layer hampered the direct contact between *At. thiooxidans* and arsenopyrite, considering a significant number of cells were observed on the oxidation layer outer surface. The attachment of acidophilic bacteria to the surface of sulfidic ores is a crucial process in Fe/S bio-oxidation, particularly in the initial stage (Tributsch,

2001). In general, indirect bioleaching by biogenic Fe^{3+} gains importance in the later stages of the mineral dissolution process. The results of this study showed a presence of a thick layer of accumulated Fe/S/As-bearing phases on the mineral surface in the BSM assay after 8 days of bioleaching (Fig. 2b). A significantly different surface structure of the arsenopyrite residue was observed in the AMD assay, with the initial fine product layer developing into structures of aggregated nanosheets (Fig. 2f).

With prolonged bioleaching (15 days), two distinctive layers were formed on the mineral residue surface in the BSM assay. The inner layer was well-crystallized, and comprised aggregated disk-like microstructures (~1 μm diameter) corresponding to jarosite. The inner layer was coated by a fine and dense outer layer composed of (wt.%): 35.4 O, 31.3 Fe, 25.8 As, 6.2 S, and 1.3 K (Figs. 2c and S4a). In the AMD assay, the morphological features of arsenopyrite were not observed on the surface of the leaching residue after 15 days, and small aggregated nanosheets were formed, with high contents of As (30.2%) and S (8.1%) (Figs. 2g and S4b). Compared to the residue from the abiotic BSM assay (shown in Fig. 2d), more extensive corrosion was observed on the surface of arsenopyrite in the AMD sterile assay (Fig. 2h). The above results indicate that AMD could be a suitable alternative to growth media used in bioleaching of sulfidic minerals. Using AMD instead of BSM could significantly reduce the costs of large-scale industrial mineral processing.

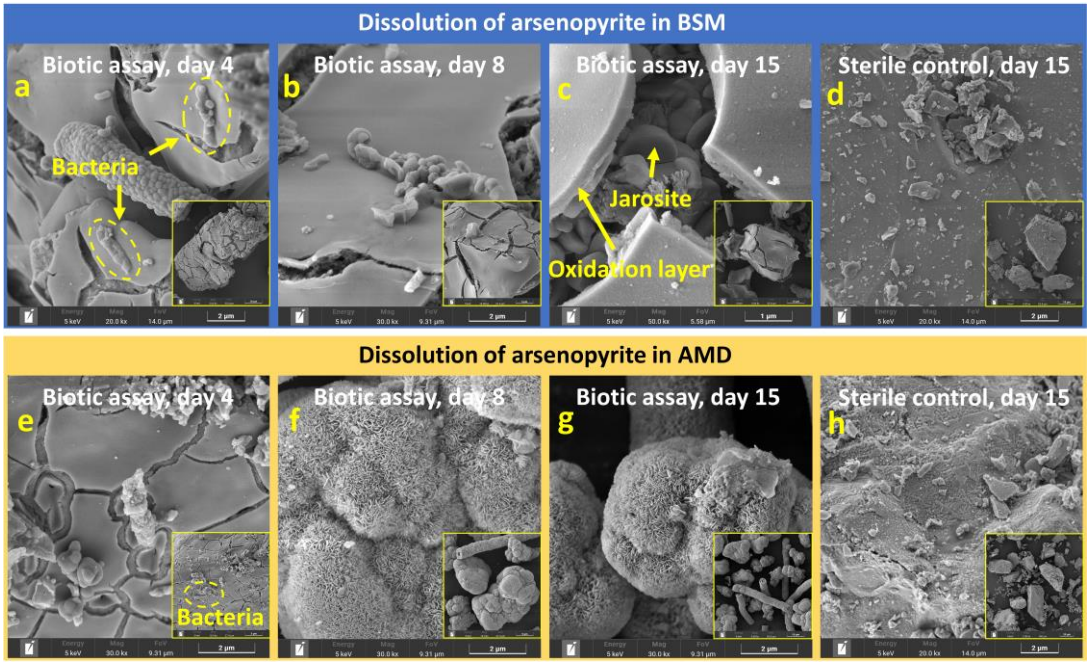

Fig. 2. SEM images of precipitates collected from (a-d) BSM and (e-f) AMD assays after 4 (a, e), 8 (b, f), and 15 (c, g) days of arsenopyrite bioleaching under aerobic conditions; SEM images of arsenopyrite residues collected from (d) BSM and (h) AMD sterile controls after 15 days.

The analysis of solids confirmed the above hypothesis, indicating a greater rate of microbially catalyzed arsenopyrite dissolution occurred in the AMD assay (Fig. 3b) compared to BSM (Fig. 3a) (both under aerobic conditions), together with more extensive accumulation of S^0 and tooeleite [$Fe^{III}_6(As^{III}O_3)_4(SO_4)(OH)_4{\cdot}4H_2O$] (Fig. 3b). The content of jarosites (mainly K-jarosite, identified by EDS; Fig. S4a) was higher in the BSM precipitate after 4 days of arsenopyrite bioleaching, compared to the AMD bioleaching assay. After 15 days of bioleaching, tooeleite, S^0 and jarosites were the dominant phases in the BSM residue, with low amounts of arsenopyrite still present (Fig. 3a). In contrast, no arsenopyrite was detected in the precipitate recovered from the AMD bioleaching system, and poorly crystalline substances were abundant in the XRD

pattern (Fig. 3b). Commonly, S^0 and jarosites are the main components of mineral passivation layers that mitigate further mineral dissolution catalyzed by bacteria and/or Fe^{3+} (Hol et al., 2011). It has been postulated that the structure of an oxidation layer has a great impact on sulfide bioleaching, including arsenopyrite (McGuire et al., 2001). In this study, the presence of the double layer on the BSM residue surface hampered the attachment of bacterial cells to and attack by Fe^{3+} on the mineral surface, resulting in arsenopyrite dissolution inhibition (as shown in the left schematic in Fig. 3c). The amorphous nanosheet structure formed on the surface of the residue in the AMD assay, on the other hand, allowed the attack of Fe^{3+} on the mineral surface, leading to significantly more extensive arsenopyrite dissolution in AMD (Fig. 3c right) compared to BSM. Only arsenopyrite phases were present in the XRD patterns of solids collected from abiotic controls (Fig. S5).

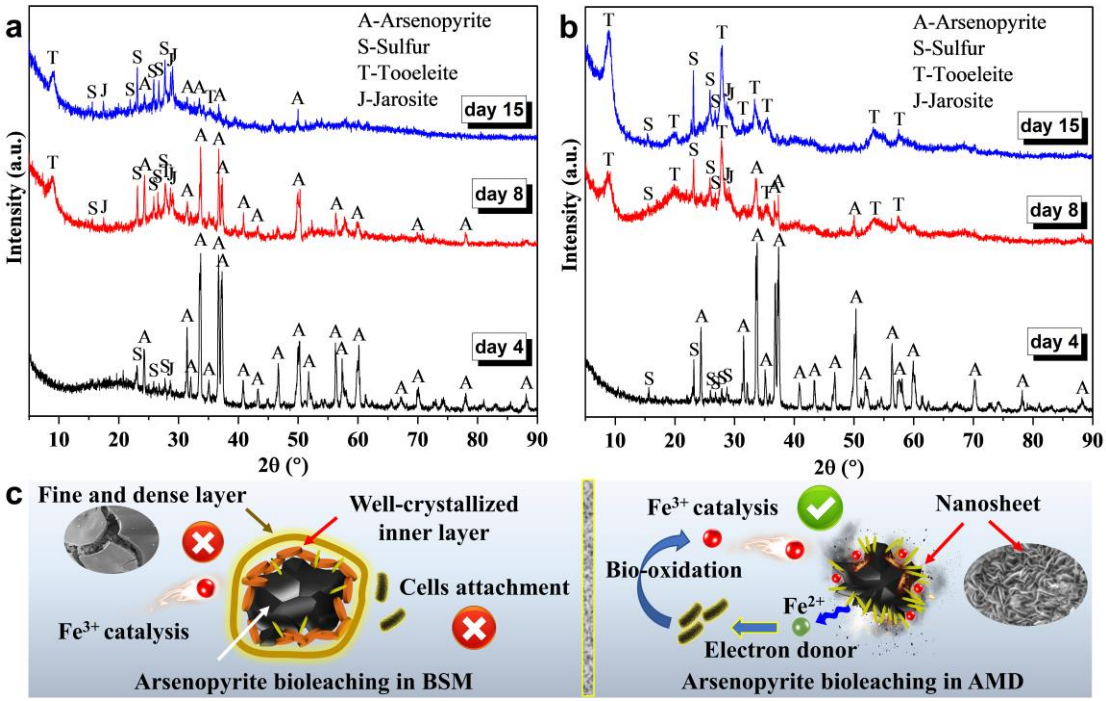

Fig. 3. XRD patterns of solid residues after 4, 8, and 15 days of aerobic arsenopyrite bioleaching in (a) BSM and (b) AMD; (c) Effects of the structure of the surface

passivation layer on arsenopyrite dissolution in BSM (left) and AMD (right).

3.3. Transformations of S, As, and Fe species in arsenopyrite bioleaching residues

Based on the S $2P_{3/2}$ spectra (Fig. 4a-d) and fitting results (Table S1), the main surface S species in the arsenopyrite residues after 4 days of bioleaching were $(AsS)^{2-}$, S_n^{2-}, S^0, and SO_4^{2-} in both BSM (Fig. 4a) and AMD (Fig. 4b). The greater proportion of S^0 (12.5%) and lower proportion of $(AsS)^{2-}$ (7.98%) in the AMD residue confirmed a greater rate of S oxidation in AMD compared to BSM. Progressing dissolution of arsenopyrite led to a decrease in the proportion of $(AsS)^{2-}$ in the BSM solids from 9.76 to 4.45% from day 4 to 15, together with an increase in SO_4^{2-} content from 59.31 to 74.07%. In contrast, the $(AsS)^{2-}$ peak was not detected in the spectrum of the residue in the AMD assay (Fig. 4d), which was in agreement with the above XRD data. The results indicate that the formation of Fe(III)-hydroxysulfate secondary minerals in BSM passivated the surface of arsenopyrite and hindered its dissolution, while this was not observed in AMD.

Significant differences were observed between the As K-edge XANES spectra of the BSM and AMD residues collected after 15 days of bioleaching (Fig. 4e). Dissimilar peak positions and intensities indicated different arsenopyrite dissolution mechanisms, and therefore As fate, were likely to occur in the two assays. A strong peak corresponding to As(III) (at 11,871.3 eV) and a weak shoulder peak for As(V) (at 11,875 eV) were observed in the AMD spectrum, showing that As precipitated in the reduced form. The LCF results indicated the tooeleite proportion was 87.5%, with only minor

contents of AFA (8.9%) and Na_2AsO_3 (3.6%) in the AMD residue (Fig. 4g). As(III) precipitation can alleviate inhibition of arsenopyrite dissolution, as well as reduce the toxic effects of dissolved As(III) on *At. thiooxidans* cells. In contrast, As(V)-bearing phases dominated in the BSM bioleaching residue, with amorphous ferric arsenate (AFA) constituting 81.1% (and tooeleite and crystalline scorodite proportions reaching 11.6 and 7.3% respectively) (Fig. 4f). Fe(III) was a dominant Fe species in both BSM and AMD solid residues (Fig. S6).

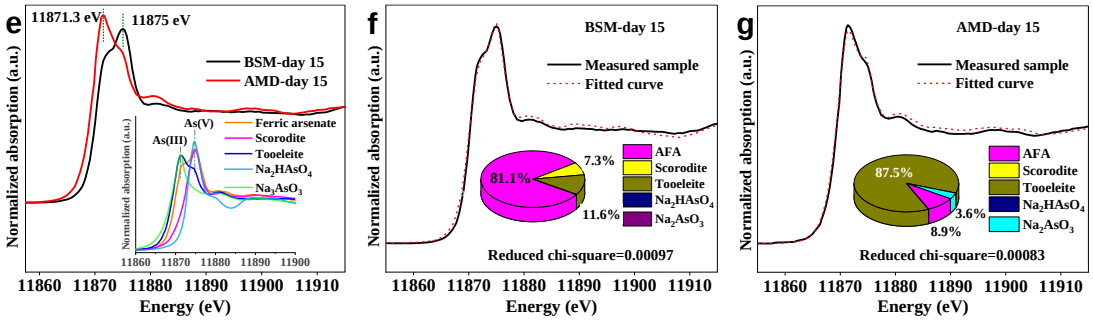

Fig. 4. (a-d) XPS spectra of S species on the surface of the residues collected from the BSM (a, c) and AMD (b, d) assays after 4 (a, b) and 15 (c, d) days of aerobic arsenopyrite bioleaching; (e) As K-edge XANES spectra of solid residues after 15 days of arsenopyrite bioleaching (together with those of As-bearing references), and LCF results for the (f) BSM and (g) AMD precipitates. Legend: AFA = amorphous ferric arsenate.

In summary, it can be concluded that AMD is a suitable substitute for culture media (such as BSM and 9K) in arsenopyrite bioleaching under aerobic conditions. The amorphous layer (composing mainly of tooeleite and minor amounts of AFA) formed on the arsenopyrite surface in AMD exhibited a permeable nanosheet structure, which did not inhibit the contact between arsenopyrite and leaching agents (i.e., Fe^{3+} and H^+),

thus enabling continuous dissolution of the mineral. In contrast, the arsenopyrite surface in BSM was completely passivated at the later bioleaching stages. The passivation layer comprised an inner layer (composed of K-jarosite and tooeleite) and outer layer (S^0 and AFA), and this structure effectively suppressed further arsenopyrite oxidation.

3.4. Sulfur oxidation coupled with BOAR reductive dissolution catalyzed by At. thiooxidans

To eliminate the Fe(III)-bearing secondary products accumulated on the arsenopyrite surface and to further improve mineral bio-oxidation rate, reductive dissolution of BOAR from the BSM assay was performed, catalyzed by *At. thiooxidans* oxidizing S^0 and $S_2O_3^{2-}$. As shown in Fig. 5a, an increase in $[Fe^T]_{aq}$, was observed during the reductive bioleaching process, indicating gradual dissolution of BOAR, with higher efficiencies achieved in assays containing 1 and 2 g/L of sulfur in the form of $S_2O_3^{2-}$, compared to assays with corresponding amounts of S^0 (Fig. 5d). A higher amount of $S_2O_3^{2-}$ (3 g S/L) did not result in a higher BOAR dissolution rate (Fig. 5d). The changes in $[Fe^{2+}]_{aq}$ (Fig. 5b), cell density (Fig. 6a), and $[SO_4^{2-}]$ (Figs. 6b, c) followed the above-described changes in $[Fe^T]_{aq}$, indicating that dissimilatory iron reduction coupled to sulfur bio-oxidation (DIRSO) catalyzed by *At. thiooxidans* enhanced the dissolution of BOAR. The changes in the concentration of solubilized As (Fig. 6d) during the reductive dissolution of BOAR tallied with the changes in Fe concentration, implying that Fe/As-bearing secondary products (i.e., $FeAsO_4$ (AFA and scorodite), and $Fe_6(AsO_3)_4(SO_4)(OH)_4{\cdot}4H_2O$), were the primary electron acceptors in

DIRSO.

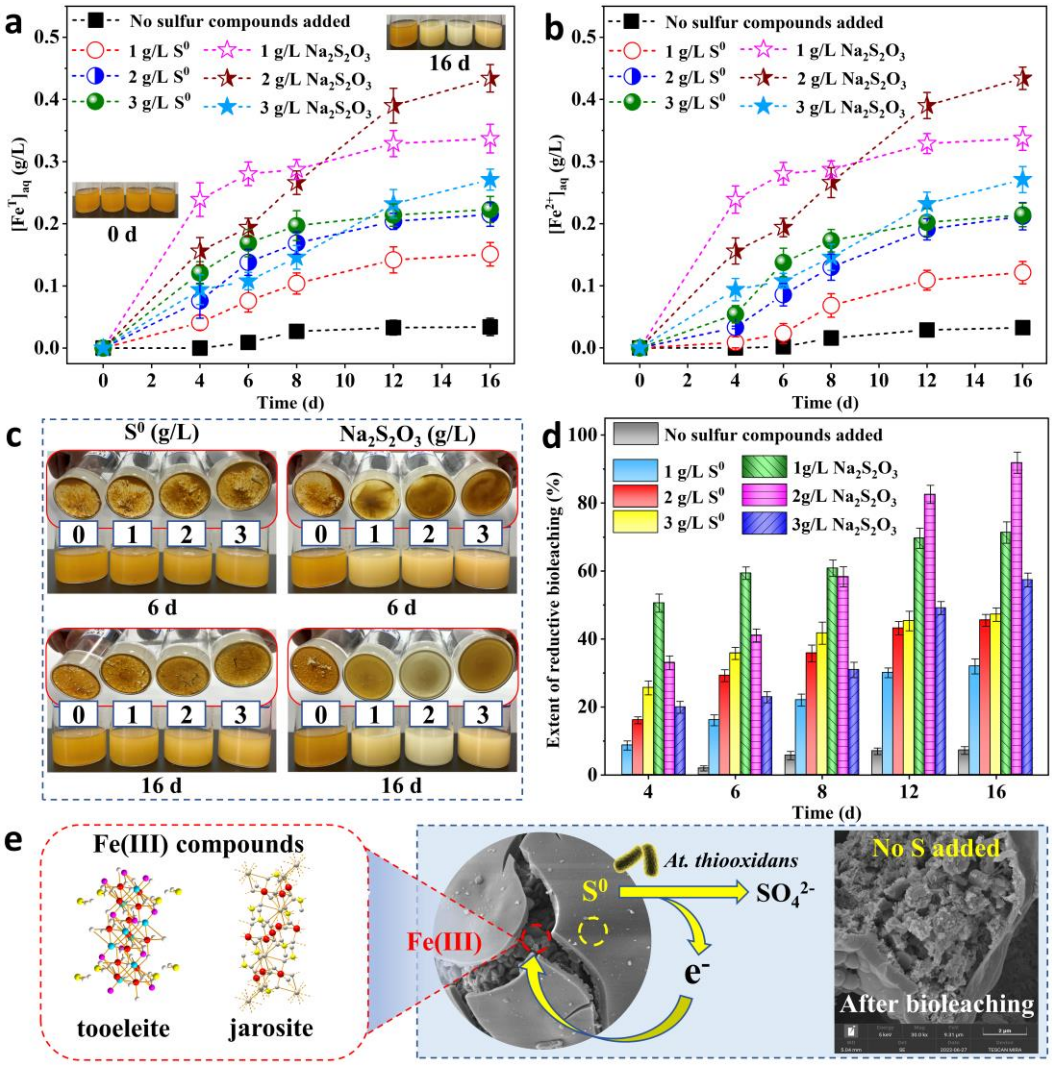

Fig. 5. Changes in (a) $[Fe^{T}]_{aq}$, (b) $[Fe^{2+}]_{aq}$, (c) color changes in the assay solutions and residues, and (d) the extent of reductive dissolution of bio-oxidized arsenopyrite residue (BOAR) under anaerobic conditions, catalyzed by *At. thiooxidans* oxidizing different concentrations of S^0 and $Na_2S_2O_3$, based on Fe dissolution data; (e) a schematic showing anaerobic dissolution of BOAR without sulfur compounds added.

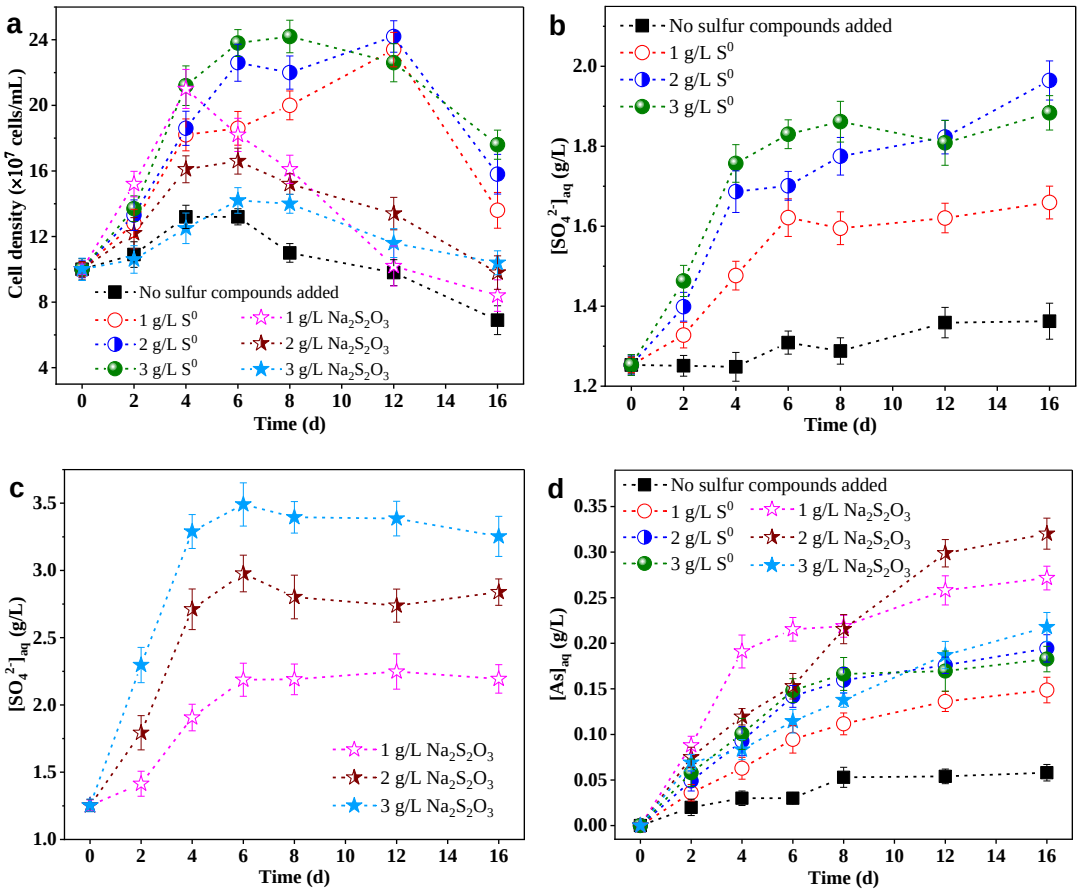

Fig. 6. Changes in (a) cell density, (b, c) $[SO_4^{2-}]_{aq}$, and (d) $[As]_{aq}$ during reductive dissolution of bio-oxidized arsenopyrite residues (BOARs) catalyzed by *At. thiooxidans* oxidizing different concentrations of S^0 (a,b,d) and $Na_2S_2O_3$ (a,c,d).

Fig. 5c shows the color changes in the anaerobic assays. The colors of the assays containing S^0 and $S_2O_3^{2-}$ became lighter after 6 days compared to those observed in the initial stage (shown in Fig. S7). The lightest color (indicating the greatest rate of reductive dissolution of BOAR) was detected in the assay with 1 g/L S ($S_2O_3^{2-}$). However, after 12 (Fig. S7) and 16 days (Fig. 5a), the most profound color change was observed in the assay with 2 g/L S ($S_2O_3^{2-}$). This was supported by dissolved Fe concentration data analyzed after 16 days, showing the dissolution of BOAR reached 71.3, 91.9, and 57.4% in assays containing 1, 2, and 3 g/L S ($S_2O_3^{2-}$), respectively.

Lower values of Fe solubilization were determined in assays with S^0 (reaching 32.0, 45.5, and 47.2%, respectively) (Fig. 5d). Both S^0 and $S_2O_3^{2-}$ are common intermediates occurring during sulfidic ore bioleaching processes (Vera et al., 2013). It has been previously described that $S_2O_3^{2-}$ can serve as an electron donor during anaerobic oxidation coupled to Fe^{3+} reduction (Chen et al., 2022). The reduced bacterial growth and BOAR dissolution observed in assays with excessive $S_2O_3^{2-}$ (3 g S/L) were ascribed to elevated pH caused by the electron donor addition.

Interestingly, in the assay without sulfur compounds, the rate of BOAR dissolution reached 7.2% in 16 days, with soluble Fe existing predominantly as Fe^{2+} (Figs. 5a, b). The intensity of the S^0 diffraction peak in BOAR XRD spectrum (Fig. S8) decreased after reductive bioleaching, correlating with the tooeleite and jarosite peak intensity decreases. The above findings indicate that *At. thiooxidans* can oxidize a portion of the S^0 present in BOAR coupled to reduction of Fe^{3+} (mainly present in tooeleite precipitated in BOAR), resulting in partial dissolution of BOAR without additional sulfur sources (Fig. 5e).

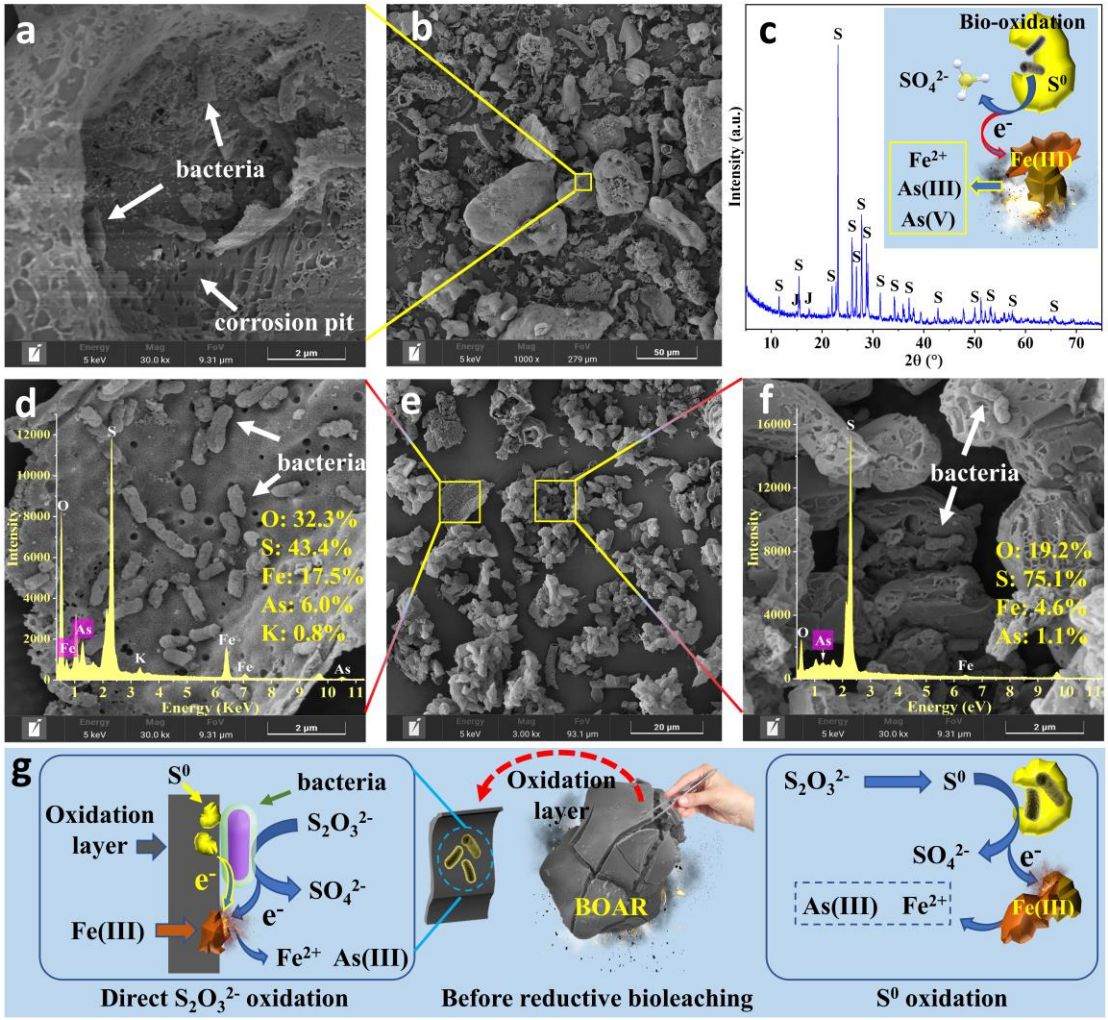

Fig. 7. (a, b) SEM images and (c) XRD pattern of BOAR residue after 16 days of reductive dissolution catalyzed by *At. thiooxidans* oxidizing S^0 (2 g S/L), together with a schematic showing the oxidation-reduction process; (d-f) SEM-EDS images of BOAR residue after 16 days of reductive dissolution catalyzed by *At. thiooxidans* oxidizing $Na_2S_2O_3$ (2 g S/L); (g) schematic diagram of reductive dissolution of BOARs by *At. thiooxidans* oxidizing $Na_2S_2O_3$, showing direct $S_2O_3^{2-}$ oxidation (left) and S^0 (generated from $S_2O_3^{2-}$) oxidation (right) processes involved.

Adsorption of bacterial cells onto the surface of S^0 particles is crucial for sulfur bio-oxidation under both aerobic and anaerobic conditions (Nguyen and Lee, 2015;

Zhang et al., 2022). Fig. 7a, b shows that in the biotic assay with 2 g S/L (S^0), extensive dissolution of BOAR was observed, with numerous corrosion pits and adhered *At. thiooxidans* cells visible on the surface of S^0 particles. A solid phase composition analysis (Figs. 7c and S10a) showed a significant decrease in jarosite content and complete absence of tooeleite after 16 days of BOAR bioleaching under anaerobic conditions. These results confirm that reductive dissolution of BOAR proceeds *via* reduction of Fe^{3+} in Fe(III)- and/or As(V/III)-bearing phases (i.e., tooeleite, AFA, scorodite, and K-jarosite) to Fe^{2+}, using electrons generated through S oxidation catalyzed by S-oxidizing chemolithotrophs, such as *At. thiooxidans* (Eqs. (6-10)). These processes disrupt the equilibrium between Fe^{3+} in solution and in the solid phase, thus accelerating BOAR dissolution (Banwart et al., 1989; Marrero et al., 2015).

$$Fe_6(AsO_3)_4(SO_4)(OH)_4 \cdot 4H_2O + 16H^+ \leftrightarrow 6Fe^{3+} + 4H_3AsO_3 + {SO_4}^{2-} + 8H_2O \quad (6)$$

$$FeAsO_4 + 3H^+ \leftrightarrow Fe^{3+} + H_3AsO_4 \quad (7)$$

$$KFe_3(SO_4)_2(OH)_6 + 6H^+ \leftrightarrow 3Fe^{3+} + K^+ + 2{SO_4}^{2-} + 6H_2O \quad (8)$$

$$S^0 + 4H_2O \xrightarrow{At.thiooxidans} {SO_4}^{2-} + 8H^+ + 6e^- \quad (9)$$

$$Fe^{3+} + e^- \rightarrow Fe^{2+} \quad (10)$$

The typical morphological features of BOAR mostly disappeared after 16 days of reductive dissolution in the biotic assay with 2 g/L S ($S_2O_3^{2-}$). Instead, irregularly shaped particles were formed composing mainly of S, with bacterial cells attached to the surface (Figs. 7e, f). Fig. 7d shows that many of the bacterial cells were adsorbed on the inside of the residual oxidation layer of BOAR (which composed of (in wt.%): 43-75 S, 19-32 O, and 5-18 Fe, with minor proportions of As and K), and corrosion pits

were observed in the vicinity of the bacteria. The predominance of S in the residual oxidation layer further confirmed BOAR dissolution. Furthermore, XRD results (Fig. S9b) indicated complete dissolution of tooeleite and jarosite in the assay with 2 g/L S ($S_2O_3^{2-}$), while the dissolution of jarosite was partially inhibited in assays with higher [3 g/L S ($S_2O_3^{2-}$)] or lower [1 g/L S ($S_2O_3^{2-}$)] sulfur contents. These results indicate that jarosite was more difficult to bio-dissolve under anaerobic conditions than Fe(III)/As-bearing compounds such as tooeleite and scorodite.

Based on the above findings, a model is suggested for BOAR dissolution *via* $S_2O_3^{2-}$ oxidation coupled to Fe^{3+} reduction, catalyzed by *At. thiooxidans* (Fig. 7g). The process follows Eq. (11), with oxidation of $S_2O_3^{2-}$ proceeding *via* S^0 (Eqs. (12, 13)). The bacterial cells then attach to the S^0 particle surface, and catalyze reduction of Fe^{3+} in BOAR.

$$S_2O_3{}^{2-} + 8Fe^{3+} + 5H_2O \xrightarrow{At.thiooxidans} 2SO_4{}^{2-} + 8Fe^{2+} + 10H^+ \quad (11)$$

$$S_2O_3{}^{2-} + 2H^+ \rightarrow H_2S_2O_3 \quad (12)$$

$$H_2S_2O_3 \rightarrow SO_2 + S^0 + H_2O \quad (13)$$

The generated Fe^{2+} and residual S^0 could be used as electron donors for acidophilic chemolithotrophs to enhance subsequent bio-oxidation of the sulfidic minerals under aerobic conditions. Such sequential bio-oxidation using alternating aerobic and anaerobic phases could facilitate improved Au extraction with efficiently eliminate unstable Fe(III)/As-bearing secondary products.

4. Conclusions

Two-step sequential bioleaching catalyzed by *At. thiooxidans* was performed to enhance arsenopyrite bio-oxidation. Firstly, an aerobic bioleaching step was performed. The oxidation layer (composing of S^0, AFA, K-jarosite, tooeleite, and scorodite) formed on the arsenopyrite surface in BSM passivated the surface and inhibited further dissolution. Improved arsenopyrite bioleaching was achieved in AMD, leading to the formation of an amorphous nanosheet structure (comprising mainly tooeleite) on the mineral surface, which did not obstruct the contact of chemolithotrophic bacteria and Fe^{3+} with the mineral. The findings show that AMD can be used as a cost-effective alternative to growth media in bio-oxidation processes. Secondly, reductive dissolution of the residual arsenopyrite was performed *via* enhanced sulfur oxidation catalyzed by *At. thiooxidans* using external S^0 and $S_2O_3^{2-}$ as electron donor under anaerobic condition. The reductive process successfully removed the passivation layer. On an industrial scale, enhanced Au extraction could be achieved *via* improved kinetics of arsenopyrite dissolution. Further research could investigate the efficiency of sequential leaching with a higher number of alternating aerobic and anaerobic phases, as well as upscaling of the two-step process. The elevated costs of a large-scale technology allowing alternating aerated and anoxic bio-oxidation steps could be reduced by the use of AMD instead of a growth medium.

Declaration of Competing Interest

The authors declare that they have no known competing financial interests or

personal relationships that could have appeared to influence the work reported in this paper.

Acknowledgements

Funding for this research was provided by the Key Research and Development Program of Hunan Province, China (2020SK2125, 2022NK2057), and the National Key Research and Development Program of China (2018YFE0110200). We would like to thank Tie-Fu Xu (Hunan Navi New Material Technology Co., Ltd.) for his assistance in micromorphology analysis.

References

Banwart, S., Davies, S., Stumm, W., 1989. The role of oxalate in accelerating the reductive dissolution of hematite (α-Fe_2O_3) by ascorbate. Colloids Surf. 39, 303-309.

Brierley, C.L., Brierley, J.A., 2013. Progress in bioleaching: part B: applications of microbial processes by the minerals industries. Appl. Microbiol. Biotechnol. 97, 7543-7552.

Brittan, M., 1995. Oxygen roasting of refractory gold ores. Miner. Eng. 47, 145-148.

Cabri, L.J., Newville, M., Gordon, R.A., Crozier, E.D., Sutton, S.R., McMahon, G., Jiang, D.T., 2000. Chemical speciation of gold in arsenopyrite. Can. Mineral. 38, 1265-1281.

Castro, L., García-Balboa, C., González, F., Ballester, A., Blázquez, M.L., Muñoz, J.A., 2013. Effectiveness of anaerobic iron bio-reduction of jarosite and the influence

of humic substances. Hydrometallurgy 131-132, 29-33.

Chai, L., Yue, M., Yang, J., Wang, Q., Li, Q., Liu, H., 2016. Formation of tooeleite and the role of direct removal of As (III) from high-arsenic acid wastewater. J. Hazard. Mater. 320, 620-627.

Chen, H.R., Zhang, D.R., Nie, Z.Y., Xia, J.L., Li, Q., Zhang, R.Y., Yin, H.H, Pakostova, E., 2022. Reductive dissolution of jarosite by inorganic sulfur compounds catalyzed by *Acidithiobacillus thiooxidans*. Hydrometallurgy 212, 105908.

Chen, M., Lu, G., Wu, J., Sun, J., Dang, Z., 2020. Acidity and metallic elements release from AMD-affected river sediments: effect of AMD standstill and dilution. Environ. Res. 186, 109490.

Datta, S., Rule, A.M., Mihalic, J.N., Chillrud, S.N., Bostick, B.C., Ramos-Bonilla, J.P., Han, I., Polyak, L.M., Geyh, A.S., Breysse, P.N., 2012. Use of X-ray absorption spectroscopy to speciate manganese in airborne particulate matter from five counties across the United States. Environ. Sci. Technol. 46, 3101-3109.

Dave, S.R., Gupta, K.H., Tipre, D.R., 2008. Characterization of arsenic resistant and arsenopyrite oxidizing *Acidithiobacillus ferrooxidans* from Hutti gold leachate and effluents. Bioresour. Technol. 99, 7514-7520.

Deng, S., He, G., Wu, B., Gu, G., 2020. Pyrite-promoted dissolution of arsenopyrite in the presence of *Sulfobacillus thermosulfidooxidans*. J. Mater. Res. Technol. 9, 9362-9371.

Duquesne, K., Lebrun, S., Casiot, C., Bruneel, O., Personne, J.C., Leblanc, M., Elbaz-Poulichet, F., Morin, G., Bonnefoy, V., 2003. Immobilization of arsenite and ferric

iron by *Acidithiobacillus ferrooxidans* and its relevance to acid mine drainage. Appl. Environ. Microbiol. 69, 6165-6173.

Hol, A., Van der Weijden, R.D., Van Weert, G., Kondos, P., Buisman,C.J.N., 2011. Processing of arsenopyritic gold concentrates by partial bio-oxidation followed by bioreduction. Environ. Sci. Technol. 45, 6316-6321.

Karamanev, D.G., Nikolov, L.N., Mamatarkova, V., 2002. Rapid simultaneous quantitative determination of ferric and ferrous ions in drainage. Miner. Eng. 15, 341-346.

Lengke, M. F., Sanpawanitchakit, C., Tempel, R. N., 2009. The oxidation and dissolution of arsenic-bearing sulfides. Can. Mineral. 47, 593-613.

Lovley, D.R., Phillips, E.J., 1987. Rapid assay for microbially reducible ferric iron in aquatic sediments. Appl. Environ. Microbiol. 53, 1536-1540.

Marrero, J., Coto, O., Goldmann, S., Graupner, T., Schippers A. 2015. Recovery of nickel and cobalt from laterite tailings by reductive dissolution under aerobic conditions using *Acidithiobacillus* species. Environ. Sci. Technol. 49, 6674-6682.

McGuire, M.M., Edwards, K.J., Banfield, J.F., Hamers, R.J., 2001. Kinetics, surface chemistry, and structural evolution of microbially mediated sulfide mineral dissolution. Geochim. Cosmochim. Acta 65, 1243-1258.

Ng, W.S., Liu, Y.H., Chen, M., 2022. The effect of curing on arsenic precipitation and kinetic study of pressure oxidation of pyrite and arsenopyrite. Miner. Eng. 185, 107675.

Nguyen,V.K., Lee, J.U., 2015. Effect of sulfur concentration on microbial removal of

arsenic and heavy metals from mine tailings using mixed culture of *Acidithiobacillus* spp. J. Geochem. Explor. 148, 241-248.

Ohmura, N., Sasaki, K., Matsumoto, N., Saiki, H., 2002. Anaerobic respiration using Fe^{3+}, S^0, and H_2 in the chemolithoautotrophic bacterium *Acidithiobacillus ferrooxidans*. J. Bacteriol. 184, 2081-2087.

Osorio, H., Mangold, S., Denis, Y., Ñancucheo, I., Esparza, M., Johnson, D.B., Bonnefoy, V., Dopson, M., Holmes, D.S., 2013. Anaerobic sulfur metabolism coupled to dissimilatory iron reduction in the extremophile *Acidithiobacillus ferrooxidans*. Appl. Environ. Microbiol. 79, 2172-2181.

Pathak, A., Morrison, L., Healy, M.G., 2017. Catalytic potential of selected metal ions for bioleaching, and potential techno-economic and environmental issues: A critical review. Bioresour. Technol. 229, 211-221.

Ramírez-Aldaba, H., Valles, O.P., Vazquez-Arenas, J., Rojas-Contreras, J.A., Valdez-Pérez, D., Ruiz-Baca, E., Meraz-Rodríguez, M., Sosa-Rodríguez, F.S, Rodríguez, Á.G., Lara, R.H., 2016. Chemical and surface analysis during evolution of arsenopyrite oxidation by *Acidithiobacillus thiooxidans* in the presence and absence of supplementary arsenic. Sci. Total Environ. 566-567, 1106-1119.

Ravel, B., Newville, M., 2005. ATHENA, ARTEMIS, HEPHAESTUS: data analysis for X-ray absorption spectroscopy using IFEFFIT. J. Synchrotron Radiat. 12, 537-541

Roberto, F.F., Schippers, A., 2022.

Rogozhnikov, D., Karimov, K., Shoppert, A., Dizer, O., Naboichenko, S., 2021.

Kinetics and mechanism of arsenopyrite leaching in nitric acid solutions in the presence of pyrite and Fe(III) ions. Hydrometallurgy 199, 105525.

Rohwerder, T., Gehrke, T., Kinzler, K., Sand, W., 2003. Bioleaching review part A: Progress in bioleaching: fundamentals and mechanisms of bacterial metal sulfide oxidation. Appl. Microbiol. Biotechnol. 63, 239-248.

Ryu, J.G., Kim, Y., 2022. Mineral transformation and dissolution of jarosite coprecipitated with hazardous oxyanions and their mobility changes. J. Hazard. Mater. 427, 128283.

Sharma, N., Eisele, T.C., 2021. Anaerobic reductive bioleaching of manganese ores. Miner. Eng. 173, 107152.

Shaw, R.A., Petavratzi, E., Bloodworth, A.J., 2013. Resource recovery from mine waste. In: Hester, R.E., Harrison, R.M. (Eds.), Waste as a Resource. Royal Society of Chemistry, Cambridge, pp. 44-65.

Tabelin, C.B., Corpuz, R.D., Igarashi, T., Villacorte-Tabelin, M., Alorro, R.D., Yoo, K., Raval, S., Ito, M., Hiroyoshi, N., 2020. Acid mine drainage formation and arsenic mobility under strongly acidic conditions: Importance of soluble phases, iron oxyhydroxides/oxides and nature of oxidation layer on pyrite. J. Hazard Mater. 399, 122844.

Tributsch, H., 2001. Direct versus indirect bioleaching. Hydrometallurgy 59, 177-185.

Vera, M., Schippers, A., Sand, W., 2013. Progress in bioleaching: fundamentals and mechanisms of bacterial metal sulfide oxidation-part A. Appl. Microbiol. Biotechnol. 97, 7529-7541.

Vikentyev, I.V., 2015. Invisible and microscopic gold in pyrite: methods and new data for massive sulfide ores of the Urals. Geol. Ore Depos. 57, 237-265.

Zeng, J., Gou, M., Tang, Y.Q., Li, G.Y., Sun, Z.Y., Kida, K., 2016. Effective bioleaching of chromium in tannery sludge with an enriched sulfur-oxidizing bacterial community. Bioresour. Technol. 218, 859-866.

Zhang, D.R., Chen, H.R., Xia, J.L., Nie, Z.Y., Zhang, R.Y., Schippers, A., Shu, W.S., Qian, L.X., 2021. Red mud regulates arsenic fate at acidic pH via regulating arsenopyrite bio-oxidation and S, Fe, Al, Si speciation transformation. Water Res. 203, 117539.

Zhang, D.R., Chen, H.R., Xia, J.L., Nie, Z.Y., Fan, X.L., Liu, H.C., Zheng, L., Zhang, L.J., Yang, H.Y., 2020. Humic acid promotes arsenopyrite bio-oxidation and arsenic immobilization. J. Hazard Mater. 384, 121359.

Zhang, D.R., Chen, H.R., Xia J.L., Nie Z.Y., Zhang R.Y., Pakostova, E., 2022. Efficient dealkalization of red mud and recovery of valuable metals by a sulfur-oxidizing bacterium. Front. Microbiol. 13, 973568.

Zhang, G., Chao, X., Guo, P., Cao, J., Yang, C., 2015. Catalytic effect of Ag^{+} on arsenic bioleaching from orpiment (As_2S_3) in batch tests with *Acidithiobacillus ferrooxidans* and *Sulfobacillus sibiricus*. J. Hazard. Mater. 283, 117-122.

Zhu, W., Xia, J.L., Yang, Y., Nie, Z.Y., Zheng, L., Ma, C.Y., Qiu, G.Z., 2011. Sulfur oxidation activities of pure and mixed thermophiles and sulfur speciation in bioleaching of chalcopyrite. Bioresour. Technol. 102, 3877-3882.